AD-A269 321

(2)

ARMY RESEARCH LABORATORY

Mechanical Properties and Microstructure of Thermomechanically Processed, High Manganese Steel

J. F. Chinella

ARL-TR-146

August 1993

DTIC
ELECTE
SEP 16 1993
S A D

93 9 15 010

93-21573

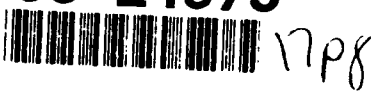

Approved for public release; distribution unlimited.

DISCLAIMER NOTICE

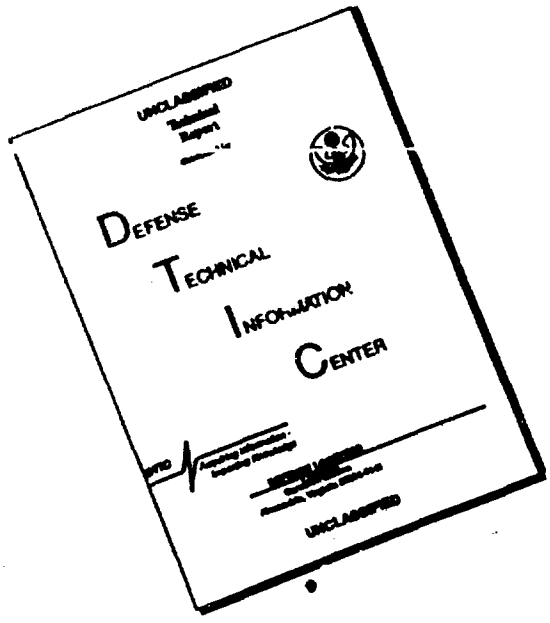

THIS DOCUMENT IS BEST QUALITY AVAILABLE. THE COPY FURNISHED TO DTIC CONTAINED A SIGNIFICANT NUMBER OF PAGES WHICH DO NOT REPRODUCE LEGIBLY.

The findings in this report are not to be construed as an official Department of the Army position unless so designated by other authorized documents.

Citation of manufacturer's or trade names does not constitute an official endorsement or approval of the use thereof.

Destroy this report when it is no longer needed. Do not return it to the originator.

REPORT DOCUMENTATION PAGE

Form Approved
OMB No. 0704-0188

Public reporting burden for this collection of information is estimated to average 1 hour per response, including the time for reviewing instructions, searching existing data sources, gathering and maintaining the data needed, and completing and reviewing the collection of information. Send comments regarding this burden estimate or any other aspect of this collection of information, including suggestions for reducing this burden, to Washington Headquarters Services, Directorate for Information Operations and Reports, 1215 Jefferson Davis Highway, Suite 1204, Arlington, VA 22202-4302, and to the Office of Management and Budget, Paperwork Reduction Project (0704-0188), Washington, DC 20503.

1. AGENCY USE ONLY (Leave blank)	2. REPORT DATE	3. REPORT TYPE AND DATES COVERED
	August 1993	Final Report - Reprint

4. TITLE AND SUBTITLE
Mechanical Properties and Microstructure of Thermomechanically Processed, High Manganese Steel

5. FUNDING NUMBERS

6. AUTHOR(S)
J. F. Chinella

7. PERFORMING ORGANIZATION NAME(S) AND ADDRESS(ES)
U.S. Army Research Laboratory
Watertown, Massachusetts 02172-0001
ATTN: AMSRL-MA-MA

8. PERFORMING ORGANIZATION REPORT NUMBER
ARL-TR-146

9. SPONSORING/MONITORING AGENCY NAME(S) AND ADDRESS(ES)
U.S. Army Research Laboratory
2800 Powder Mill Road
Adelphi, Maryland 20783-1197

10. SPONSORING/MONITORING AGENCY REPORT NUMBER

11. SUPPLEMENTARY NOTES
Published in the Conference Proceedings, High Manganese High Nitrogen Austenitic Steels, ~~ed., R. A. Lula, Metals Park, OH: ASM International~~, 1993, ~~ISBN: 0-87170-482-X~~, p. 143 - p. 153.

12a. DISTRIBUTION/AVAILABILITY STATEMENT
Approved for public release; distribution unlimited.

12b. DISTRIBUTION CODE

13. ABSTRACT (Maximum 200 words)

Thermomechanical treatments (TMT's) were performed on an austenitic Fe-12.5Mn-2.0Mo-1.15C Hadfield steel to achieve a material with high strength and resistance to plastic instability. Mechanical properties were evaluated by tensile deformation; microstructures and deformation modes were evaluated by optical or electron microscopy. Solution treated 16-18 Rockwell C hardness (HRC) material was warm rolled to a hardness of 39-53 HRC. During tensile deformation, strain hardening occurred with increasing loads and high uniform elongations to ultimate strengths equivalent to 56-57 HRC. Microstructures and deformation modes resemble those attributed to austenitic steels and other face centered cubic alloys with low to moderate stacking fault energy. Deformation was localized within grains in a orientation dependent crystallographic manner, often concentrated within bands consisting of slip and twinning. Substructures and microcracks were often restrained to grain size scale.

14. SUBJECT TERMS	15. NUMBER OF PAGES
Austenite, Deformation, Fracture, Manganese steels, Mechanical properties, Thermomechanical treatment	15
	16. PRICE CODE

17. SECURITY CLASSIFICATION OF REPORT	18. SECURITY CLASSIFICATION OF THIS PAGE	19. SECURITY CLASSIFICATION OF ABSTRACT	20. LIMITATION OF ABSTRACT
Unclassified	Unclassified	Unclassified	UL

NSN 7540-01-280-5500

Standard Form 298 (Rev. 2-89)
Prescribed by ANSI Std. Z39-18
298-102

MECHANICAL PROPERTIES AND MICROSTRUCTURE OF THERMOMECHANICALLY PROCESSED, HIGH MANGANESE STEEL

J.F. Chinella
U.S. Army Research Lab.
Watertown, MA

Abstract

Thermomechanical treatments (TMT's) were performed on an austenitic Fe-12.5Mn-2.0Mo-1.15C Hadfield steel to achieve a material with high strength and resistance to plastic instability. Mechanical properties were evaluated by tensile deformation; microstructures and deformation modes were evaluated by optical or electron microscopy. Solution treated 16-18 Rockwell C hardness (HRC) material was warm rolled to a hardness of 39-53 HRC. During tensile deformation, strain hardening occurred with increasing loads and high uniform elongations to ultimate strengths equivalent to 56-57 HRC. Microstructures and deformation modes resemble those attributed to austenitic steels and other face centered cubic alloys with low to moderate stacking fault energy. Deformation was localized within grains in a orientation dependent crystallographic manner, often concentrated within bands consisting of slip and twinning. Substructures and microcracks were often restrained to grain size scale.

AUSTENITIC, FE-MN-C HADFIELD STEEL [1-3] strain hardens to large plastic strains without plastic instability or fracture [4] over a wide range of temperatures. The exceptional toughness, work hardening capacity, and resistance to high stress abrasive wear of Hadfield steel has benefited the mining, mineral processing, earth moving equipment, and railroad industries for over a century. Recently developed austenitic manganese alloy steels also serve in cryogenic and non-magnetic applications for the power generation, transportation, and nuclear industries [5].

The standard solute composition ranges of Hadfield steel include 11.00-14.00% Mn, and 1.05-1.35% C as specified by ASTM A-128 [2]. Mo-modified Fe-12.5Mn-2.0Mo-1.15C Hadfield steel retains the toughness and strain hardening behavior of the standard alloy, avoids microvoid coalescence from detrimental carbide structures [2,6], and when decarburized, resists embrittlement through avoidance of large amounts of strain induced martensite [7,8]. The normal method of processing is a solution treatment at 1,000°C to 1,090°C for 1 to 2 hours followed by a water quench. One disadvantage, often addressed by developmental efforts, is the relatively low yield stress in the soft solution treated condition [2,5].

Hadfield steel is known to deform mainly by slip and twinning [9,10]. Under dynamic conditions, high stresses and strain rates tend to favor twinning over slip [6]. At high temperatures the kinetics for twinning in austenitic steels are favored over those for strain induced martensitic transformation [11,12,13]. Furthermore, a recent study by Adler, Olson, and Owen [13] has modeled strain hardening behavior of Hadfield steel in much the same manner as the strain induced martensitic transformation in other austenitic steels. Olson [12] suggests the low temperature sensitivity of twinning may be more applicable to high strength steels utilizing the TRIP phenomena. Such a steel could provide high strength from prior thermomechanical treatment (TMT). During deformation in service, strain hardening could continue to high strains without plastic flow instability or fracture.

A material with high levels of strength and hardness, with a high capacity for work hardening over wide ranges of temperature, could provide resistance to failure modes related to flow localization or plastic instability under dynamic conditions [14-16]. This material could provide a superior armor material that may resist the thermoplastic shear instabilities that lead to a loss of load carrying capacity during ballistic penetration [16].

Consequently, the purpose of this experimental study is to apply a warm (near the recovery temperature) roll TMT [17,18] to obtain a high yield strength, a high rate of strain hardening from slip and twinning, and a high threshold of plastic instability and fracture.

Background. Although studies investigating microstructures and strain hardening of austenitic Fe-Mn Hadfield steel have reported strain induced hexagonal close packed (HCP) ε' martensites [9,19], most recent studies [9,10,13,20] associate strain hardening mainly with stacking faults, dislocations, and deformation twins. Martensitic transformations generally are not believed to occur significantly in steels with the Hadfield steel composition even

DTIC QUALITY INSPECTED 1

A-1 20

at low temperatures [1-3,7,9,10,13,20]. The hardness and strain hardening mechanisms of Hadfield steel have been related to total defect density [9,17,18], strain aging or pinning of dislocations [9,20], and the grain refinement of the austenite matrix by deformation twins [10,13,21]. Many studies demonstrate that the behavior of Fe-Mn alloys that contain interstitials is dependent on thermally activated mechanisms that influence slip and twinning [3,20,22-25]. A recent study [13] theoretically related hardening to interstitial atoms trapped during twinning—similar to lattice distortions of BCT martensites. The above studies have resulted in controversy, so that the strain hardening mechanisms of Hadfield steel are not yet fully understood [5,13,20,21].

Materials, Approach, and Experimental Procedure

Materials and Approach. Material for the study was prepared from an argon oxygen decarburized (AOD), continuous cast, 75 mm diameter ingot. The chemical analysis of the alloy (see Table I) meets ASTM A128-E2.

Table I. Chemical Analysis (Weight %)

Mn	Mo	C	Si	Cr	Al	P	S
12.5	2.01	1.15	0.73	0.33	<0.05	<0.03	0.001

Figure 1 outlines the processing procedure. Because the microstructures of warm rolled and strained in tension material are likely to be complex and difficult to interpret, the experimental procedure included observations of material deformed to low strains.

Fig. 1 Processing Procedure.

Initial condition: 75 mm dia., AOD continuous cast ingot.

- Prepare: Austenitic, Solution Treated Bar
  (Reference material)
  (a) Forge, Solution treat 1030 °C 1 hr., Water quench
- Prepare: Austenitic, Bar Stock for TMT
  (a) Rough forge bar, Water quench,
  (b) Paint with ceramic, Soak 1,120°C 20 hrs, Water quench
  (c) Finish forge 1,040°C, to 3.56 x 2.23 cm bar
  (d) Sol. treat 1 hour at 1030-1040°C, Water quench
  (e) Condition bar (l,w,t) to 8.1-8.9 x 3.38 x 1.96 cm
- Warm roll TMT
  (7-15% Reduction/pass, electric furnace, in air)
  TMT Temperature. 343, 400, 454°C (see Table II)

Solution treated material was strained in tension to fracture to observe the strain hardening behavior and mechanical properties. A section taken from the gage-length/shoulder section was examined by optical microscopy. This examination revealed the initial structures formed at low strains, to serve as a reference for more highly strained, complex microstructures after TMT and TMT followed by strain in tension.

Warm rolled material was examined by transmission electron microscopy (TEM) to provide information about substructural deformation and hardening mechanisms at one particular condition. The effects of TMT on microstructure as a function of increased temperature or effective strain were observed by optical microscopy. This trend analysis revealed the evolution from the more simple to the more complex microstructures. The more complex microstructures result from higher strains and temperatures—the TMT conditions that would more likely result in the high strengths of interest.

Tensile tests were used to determine values of strength and ductility before and after TMT. TEM and optical microscopy of warm rolled and strained in tension material, identical to that as observed after TMT, was used to characterize the material.

Fracture initiation of a representative failed specimen was studied in profile by optical microscopy and by surface examination with scanning electron microscopy (SEM). This analysis provided information about plastic instability and fracture.

Procedure. Two tension specimen sizes were used depending on bar length: (1) 0.572 cm gage diameter, with a reduced-section length of 3.175 cm; or (2) 0.406 cm gage diameter, with a reduced section length of 2.54 cm. Percentages of elongation were obtained from gage lengths that had a 4 to 1 gage length to diameter ratio geometry.

Tension tests were conducted to fracture at 23°C at a constant cross-head speed of 0.051 cm per minute. Engineering strains were recorded by extensometers up to 0.06-0.12 strain, and from then on were calculated from cross-head displacement readings. The true stress-strain values recorded at maximum load are true uniform stress (σ_u) and true uniform strain (ε_u) [4]. Knoop (500 g) microhardness tests of tensile specimen sections deformed in uniform strain verified and correlated strain hardening to values of equivalent ultimate tensile strength and Rockwell C hardness (HRC). Carbon analysis of tension specimens by the LECO combustion method and lattice parameters [26] obtained from X-ray diffraction revealed that no significant decarburization had occurred during processing.

Optical metallography included material from tensile specimens and bar sections oriented perpendicular to the rolling plane and parallel to the rolling direction (longitudinal transverse). After mechanical polishing, specimens were electropolished with a solution of 80 grams Na_2CrO_4 in 420 ml of glacial acetic acid, at 30-36 V for about 2 to 3 minutes at 23°C [27]. Specimens were electroetched in sodium chromate-glacial acetic acid solution at 5-10 V at 23°C for 5-10 minutes, or in 10-20% HCl-methanol at 4-6 V for 4-15 seconds.

TEM specimens were prepared from grip and gage lengths portions of a tensile test specimen. The TEM specimen blanks were cut perpendicular to the rolling direction by a low speed saw, then carefully ground to approximately 125 μ thickness. TEM foils were prepared with a dilute perchloric acid solution in ethanol, butoxyethanol, and distilled water in a twin jet electropolisher at 30 V and -30°C.

Experimental Results and Discussion

Microstructures of Solution Treated Material after Strain in Tension—FCC Slip and Twinning. Like Hadfield steel, other FCC alloys (Cu-8Al [28], and Cu [29] or Ag alloys [30] at low temperatures) of low to moderate

stacking fault energy (SFE) deform by slip and twinning. Awareness of the slip and twinning modes in single crystals of these alloys in tension may help to interpret the microstructures of Hadfield steel.

The initial orientation to load axis determines whether single or multiple modes of deformation systems are first activated [6]. Slip and more cellular kinds of dislocations predominate around <001> orientations. Elsewhere, deformation modes may include more planar slip and twinning on primary, conjugate, cross, and critical systems [28,29]. This orientation dependence of structural development can also be present in polycrystalline material at low strains since the compatibility strains are small and critical stresses may not be initially achieved for all potential systems [28,29,31]. Since cross slip and recovery is limited in these alloys, the initially formed microstructures may persist to high strains.

The experimental microstructures of an as-solution treated, tension specimen after a small amount of strain is shown in Figure 2. The amount of true strain of this gage-length to gage-shoulder section is estimated among 0.03 to 0.08, by comparison to a previous study of stress-strain behavior [13]. The appearance of several grains suggests twins may form along primary, conjugate, and cross slip systems [28,29]. Particular twins that appear to be unaccompanied by glide suggest a twin mode of deformation that is less dependent on slip [32,33]. Grain boundary inclusion features observed in Figure 2 are characteristic of the electropolishing of undissolved carbides.

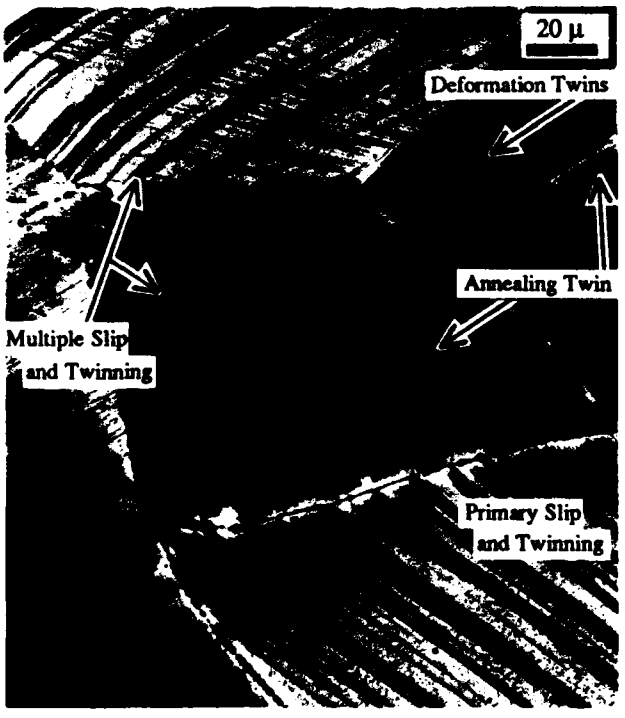

Fig. 2 Microstructural response in tension of solution treated, Fe-12.5Mn-2.0Mo-1.15C Hadfield steel. The structure includes primary and secondary deformation twins. Annealing twins from recrystallization are also shown. Low strain, gage length-gage shoulder region (0.03-0.08 ε). HCl etch -30°C.

Tension Test Results—As Solution Treated Material. Engineering stress-strain (s-e), and true stress-strain (σ-ε) curves for the Mo-modified solution treated Hadfield steel of this study (see Figure 3) are similar to previous results [1,3,13]. Deformation to high values of uniform strain occurs with increasing loads to the onset of plastic instability, necking, and fracture. The equivalent true stress-strain curve, drawn only to true uniform strain ε_u, demonstrates a region of increasing strain hardening rate ($d\sigma/d\varepsilon$) with upward curvature, reported previously to be analogous to strain hardening phenomena of Transformation Induced Plasticity (TRIP) [12,13].

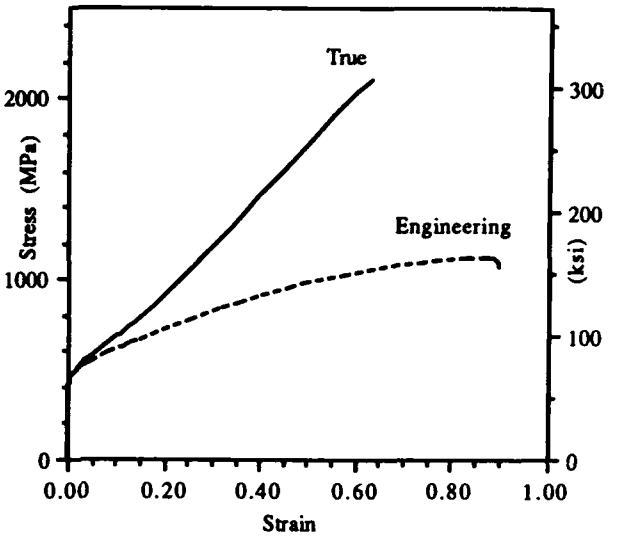

Fig. 3 Engineering s-e to fracture, and true σ-ε curves in tension to uniform strain (ε_u) at maximum load. True strain beyond maximum load is not shown. Material solution treated 1 hr. at 1,030-1,040°C.

Effects of Thermomechanical Treatment Temperature and Strain on Hardness. Table II lists the HRC values as a function of warm rolling temperature, effective strain (ε_e), and equivalent reduction of thickness (RT). Hardness increases from the initial 16-18 HRC with increasing TMT strain, and decreases slightly with increasing TMT temperature.

Microstructures after Thermomechanical Treatment. Substructures examined by TEM revealed dislocations and twin structures. After 0.46 ε_e TMT at 454°C, the substructure in a region of a particular grain (see Figure 4) consisted of dislocation tangles [17,18]. A different grain of this specimen (see Figure 5) deformed mainly by twinning and slip [34-36].

Material warm rolled at 454°C (see Figure 6) likely contains deformation bands composed mainly of slip and twin structures, as suggested by Figures 4-5 and previous studies [27-29]. The number of deformation bands in each grain are dependent upon orientation to the load axis. At low 0.29 and 0.46 effective strains, the deformation bands are relatively more distinct than after 0.75 ε_e or where band width increased. The numbers of the bands increase with increasing strain

among these samples. The numbers of the bands decrease, and the bands become more broad and indistinct, with increasing TMT temperatures for nominal 0.75 ε_e at 343, 399, and 454°C.

The broader, less distinct appearing bands, and a corresponding decrease in hardness for the higher TMT temperatures (see Figure 6 and Table II) is consistent with a greater probability for thermally activated mechanisms to assist slip and recovery. The fact that the warm rolled structure contained dislocation tangles (rather than recovered cell structure) is consistent with a limited amount of recovery that allows a high dislocation density and strain hardening during TMT [17,18].

Table II. Warm Roll TMT Hardness Values

TMT Temp. (°C)	Thickness Reduction RT(%)	Eff. Strain ε_e	Hardness HRC
343°	41	0.57	48.7
	*49	0.73	51.0
	58	0.93	53.2
399°	38	0.52	47.2
	*48	0.70	49.5
	54	0.85	51.0
	59	0.96	52.0
454°	23	0.29	39.1
	*35	0.46	45.3
	*50	0.75	49.7
	*61	1.00	52.2

*Tension Specimens Tested (see Table III)

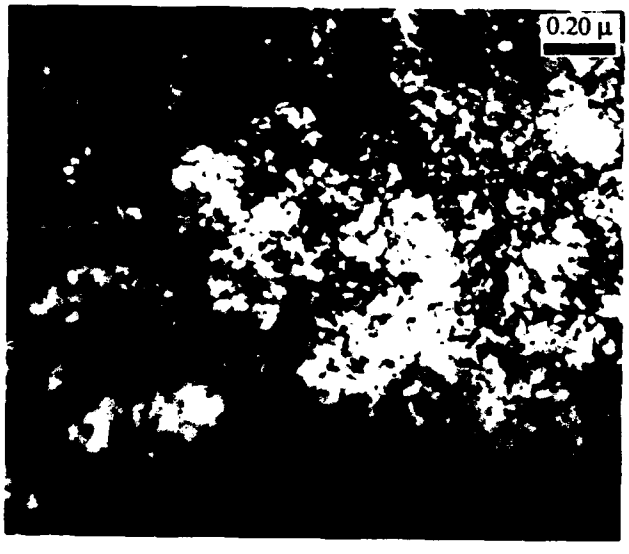

Fig. 4 Substructure exclusively composed of dislocation tangles suggests that limited amounts of recovery maintained high dislocation densities and strain hardening during experimental 0.46 ε_e TMT at 454°C. Imaged with [110] zone axis. This zone axis is parallel to the roll direction and is out of the plane of the paper.

Fig. 5 (a) Microtwin substructure formed after 0.46 ε_e TMT at 454°C. Bright field image.

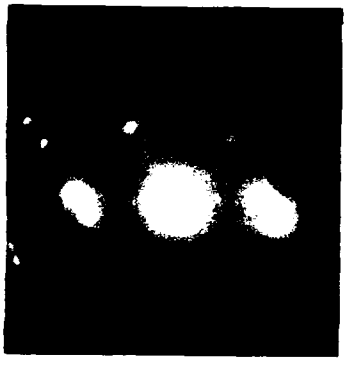

Fig. 5 (b) Electron diffraction pattern of (a).

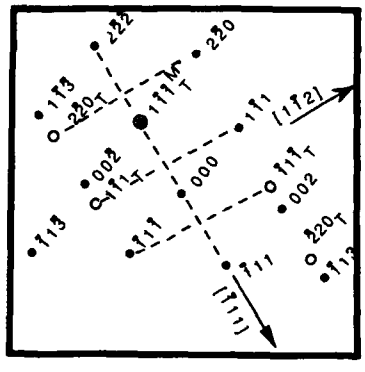

Fig. 5 (c) Predicted pattern for matrix (M) and twinned material (T) of (b), $[110]_M$ and $[\bar{1}\bar{1}0]_T$ normal to foil, consistent with twinning rotation 180° about the $[\bar{1}11]$ direction [34-36]. Not shown is the dark field micrograph imaged from the reflection indicated by the beam blocker.

A previous study of Hadfield steel [20] reported an absence of deformation twins formed in tension at quasi-stable rates at temperatures exceeding 225°C. However, material in this study deformed with high strain increments up to 454°C by twinning and slip (see Figures 4-6).

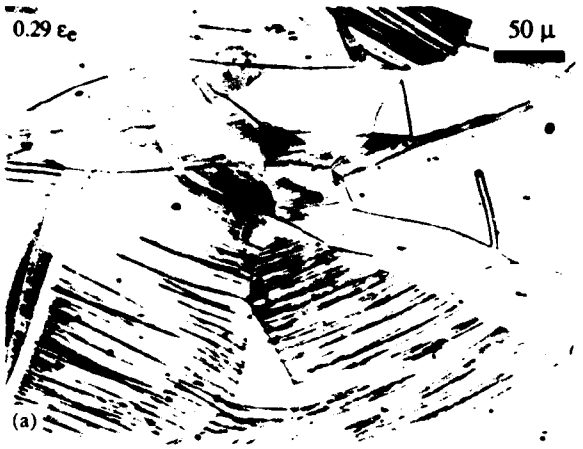

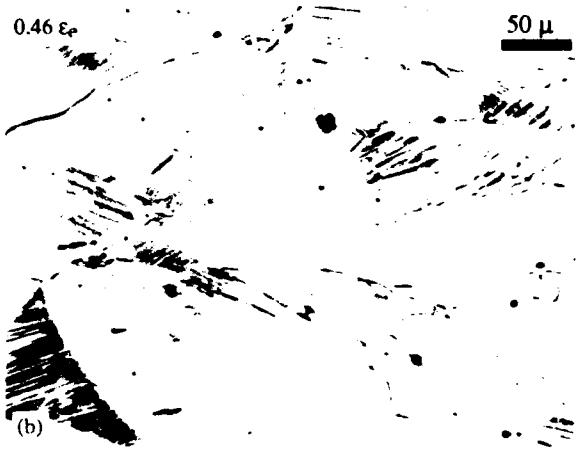

Fig. 6 (a)-(c) Structural response as a function of effective TMT strain (ε_e) at 454°C. The number of twins increase with increasing strain. (a) Structures in lower-left region suggest twin bands (see Fig. 2 and [32]). After 0.29 ε_e, structures remain somewhat discrete and crystallographic. (c) At 0.75 ε_e structures are more broad and indistinct, suggesting twin growth, top and bottom. Sodium chromate, acetic acid etch favors coarse twins [27].

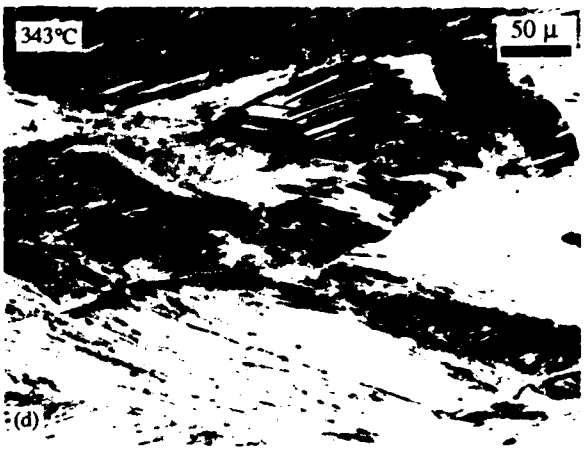

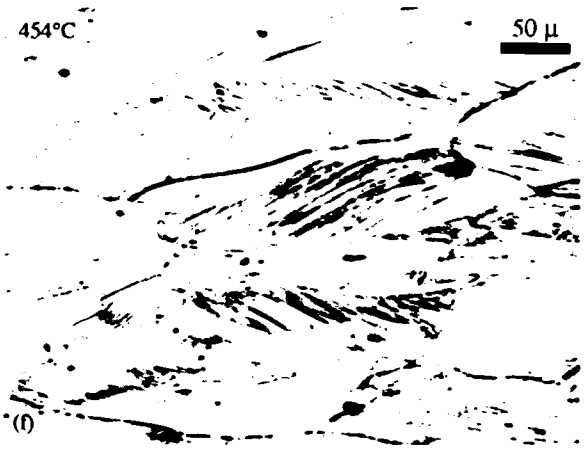

Fig. 6 (d)-(f) Structural response as a function of TMT temperature at 0.70-0.75 ε_e. Structures are more broad and indistinct at higher TMT temperatures suggesting an increased ability for slip. Sodium chromate, acetic acid electrolytic etch.

That the amount of recovery is limited, and slip and twinning occur up to about 454°C, is consistent with the large temperature ranges and high strain rates where austenitic

Fe-Mn slip-twinning alloys demonstrate superior strength, toughness, and ductility [2,9,13,23,25,37].

Previous references or studies [13,20,27] often interpret Hadfield austenitic steel structures simply as twins. The observations of this study suggest many prominent striations in deformed solution treated material resulted from twinning along slip systems—primary or conjugate twinning [28,29]. A mode of deformation by a twinning mechanism less dependent on slip may relate to the twins or deformation bands that were unaccompanied by crystallographic glide (see Figures 2,6 and [32,33]).

When slip precedes or accompanies twinning, thermally activated mechanisms [6] may control the rate or extent of twinning by limiting the nucleation, growth, or accommodation of twins. Therefore twinning is not likely to be a strictly temperature insensitive deformation mechanism—particularly in FCC Fe-Mn interstitial alloys [23-25].

Tension Test Results—Warm Rolled Material. Tensile engineering stress-strain curves, plotted to fracture, are shown in Figures 7-8. The engineering curves show that loads increase to high strains before the onset of plastic instability associated with necking and fracture. Strength increases and uniform ductility decreases with increasing amounts of TMT ε_e (see Figure 7) for the nominal 454°C warm rolled conditions. Strength decreases slightly with increasing TMT temperature (see Figure 8) for the approximately 0.75 ε_e warm rolled material, consistent with the hardness results of Table II. The values of the true local necking strains, (ε_n) [4], for this material were low even in the solution treated condition.

Table III lists the average data values of two specimens by engineering and true stress-strain. All true uniform tensile stress values of warm rolled material exceed those of the solution treated material. The greater tensile ductility for warm roll temperatures of 399°C and 454°C suggests that TMT may be more beneficial in maintaining toughness in Hadfield steel than cold working to an equivalent hardness.

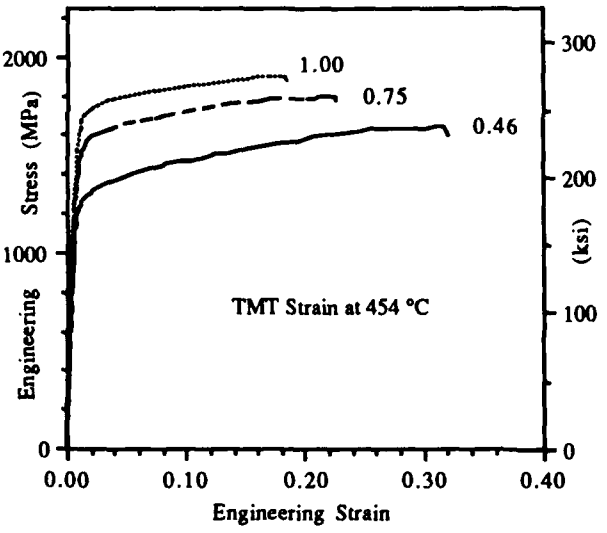

Fig. 7 Engineering s-e curves to fracture as a function of TMT strain at 454°C. Strength increases, but uniform strain in tension decreases with increased TMT strain.

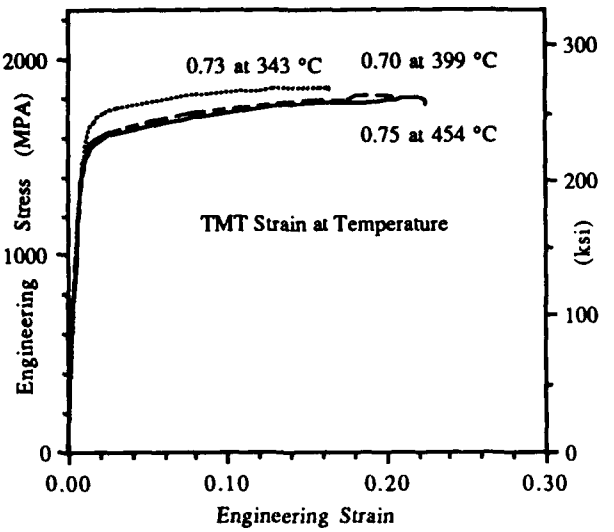

Fig. 8 Engineering s-e curves to fracture as a function of TMT temperature at 0.70-0.75 ε_e. TMT temperature has little effect on strength but a somewhat greater effect on uniform strain.

Microstructure of Thermomechanically Processed, Tension Tested Material. When examined by electron microscopy, material rolled 0.46 ε_e at 454°C, then strained in tension an additional 0.27 ε_u, revealed numerous deformation band and crystallite structures of varied morphology that ranged in thickness from 100 to less than 5 nm. Particular substructures (see Figure 9) like the grains themselves, include crystallographic primary, and secondary deformation systems and local shear displacements. Crystallite structures shown in Figures 9 and 10 suggest the possibility that twins or martensites may form within, or as, fine deformation bands at high strains in the warm rolled condition [25,38,39,40]. Crystallite substructures may also form by dynamic recovery and recrystallization [14,32,41-44].

An X-ray diffraction scan of material with 0.46 ε_e at 454°C + 0.27 ε_u in tension failed to reveal any strain induced martensitic phases.

Optical microscopy (see Figure 11), clearly revealed structures formed by orientation dependent deformation modes within grains. Although this structure was etched at approximately -30 °C, no significant differences were observed on other specimens etched at 23°C. Precise interpretations of highly strained microstructures are difficult since the structures are dependent on load axis, compatibility requirements within grains or deformation bands, and specimen orientation [31].

Microscopic shear bands (deformation bands) in general, describe planar regions of inhomogeneous strain concentrated by discrete mechanisms such as slip, twinning, or martensitic transformation. Slip dominated varieties may form in low to moderate SFE alloys after hardening by the initial slip and twinning deformation mechanisms [32,42,43]. The shear band structures in low to moderate SFE alloys are complex and include dislocations, slip bands, stacking faults, mechanical twins, and subgrain or crystallite substructures of matrix or martensitic material [32,39,40,43-46].

The appearance of most banded substructures that were observed by optical microscopy suggested crystallographic

dependent deformation modes of slip and twinning along primary, conjugate, and cross systems (see Figure 11-left, right; and [27-29,43,44]). Other substructures shown (see Figure 11, center) suggest they are deformation modes possibly formed by mechanisms of slip or strain induced martensite [32,39,42-44].

Fig. 9 Substructure following 0.46 ε_e TMT at 454°C and 0.27 ε_u in tension at 23°C.

Previous studies report that the mechanisms active in individual microsize shear bands that undergo structural transformations or recovery initially provide a local softening or a reduction in the rate of local strain hardening [42,43]. Other examples of softening effects are the local strain hardening rate reduction from primary slip-twinning and/or the softening from conjugate twinning [28,29]. Martensitic transformation of single crystallite variants in shear bands can provide easy slip between the initial and transformed structure [45]. Substructures of some crystallites in single phase alloys that are aligned with preferred orientations suggest they initially are easy paths for dislocation glide [43]. Strain hardening of the active mechanisms can occur after shear bands and crystallite variants form on secondary deformation systems, again a hardening effect like that of grain refinement [10,43,45].

Fig. 10 Substructure following 0.46 ε_e TMT at 454°C and 0.27 ε_u in tension at 23°C. Blocky crystallite substructures within bands indicate possible strain induced BCC martensite. The substructures within bands and the areas bound by bands suggests the formation of mosaic structures and texture development [36].

The present TEM and optical microscopy results (see Figures 9-11) suggest, but do not conclusively prove, that microsize shear bands are capable of replacing the initial slip and twinned structure by either slip, twinning, or strain induced martensite. Therefore twins and twin bands may not alone have provided a dominant deformation and strain hardening mechanism after TMT.

Microscopic shear bands in low to moderate SFE alloys may act as deformation modes and may be constrained to grain-size scale (see Figure 11 and [14,32,42-44]). Constraint of

Table III. Tension Test Results as a Function of TMT**

TMT T (°C)	TMT ε_e	0.2% Y.S. (MPa)	U.T.S. (MPa)	e_f	El. (%)	R.A. (%)	σ_u (MPa)	ε_u	σ_f (MPa)	ε_f	ε_n
*	*	451	1,140	0.89	77	51	2,087	0.63	2,080	0.69	0.06
454	0.46	1,154	1,653	0.32	28	27	2,155	0.26	2,176	0.30	0.04
454	0.75	1,404	1,794	0.22	23	20	2,160	0.18	2,218	0.23	0.05
454	1.00	1,587	1,900	0.18	16	17	2,216	0.16	2,237	0.17	0.01
454	0.75	1,404	1,794	0.22	23	20	2,160	0.18	2,218	0.23	0.05
399	0.70	1,400	1,814	0.22	22	20	2,172	0.18	2,222	0.22	0.04
343	0.73	1,456	1,821	0.18	20	16	2,128	0.16	2,143	0.18	0.02

* solution treated condition.
ε_e = warm roll effective strain.
T = warm roll temperature.
e_f = engineering strain to fracture.
e = engineering strain to max. load.
El. = % elong. of 4/1 length/diameter.

σ_u = true uniform stress = (P/Ao)(1+e),
ε_u = true uniform strain = ln(1+e),
σ_f = true fracture stress = P/A_f,
ε_f = true fracture strain = $2\ln(d_o/d_i)$.
ε_n = true local necking strain = $(\varepsilon_f - \varepsilon_u)$.

P = load.
A_f = area at fracture.
d = initial and final diameter.

(**Data is a··rage of 2 specimens. Mean averages & standard deviations of specimen variations: UTS: 22, 17 MPa; e_f: 0.143, 0.01.

Fig. 11 Orientation dependent microstructures and deformation bands formed in response to 0.46 ε_e TMT at 454°C followed by 0.27 ε_u in tension at 23°C. White or light etching deformation bands suggest that slip, twins, or strain induced martensites replaced the initial slip-twin structure. The arrest of slip and twin mechanisms near grain or deformation band boundaries is consistent with hardening. HCl electrolytic etch -30 °C.

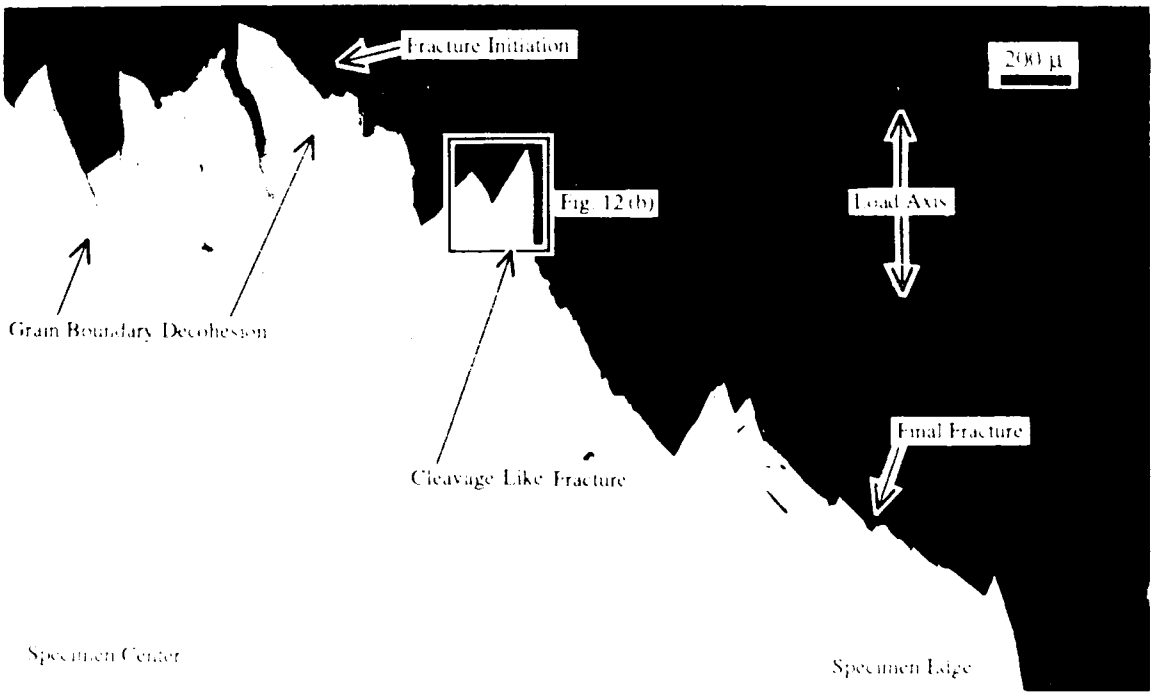

Fig. 12 (a) Fracture initiation region is distinguished by mixed mode intergranular grain boundary decohesion and transgranular microcracking. Final fracture region indicates catastrophic transgranular shear, mainly independent of decohesion and microcracking along grain boundaries or shear bands. Condition: 0.75 ε_e TMT at 454 C + 0.19 ε_u in tension at 23°C. Nital-HCl alternating etch [27] reveals general structure.

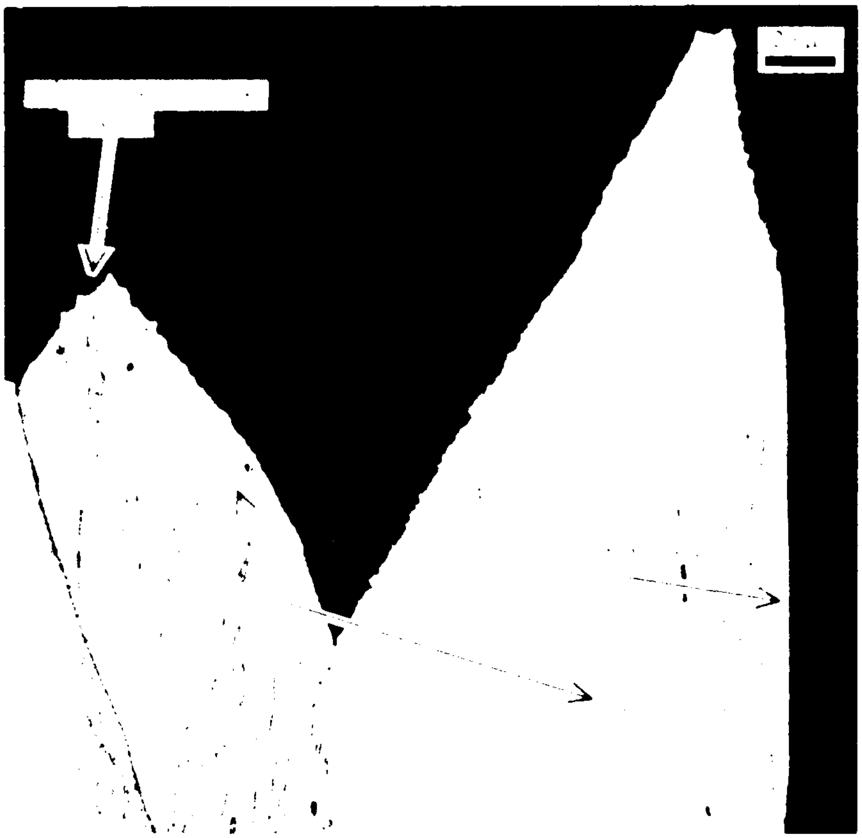

Fig. 12 (b) Two unambiguous cases of cleavage like microcracking independent of microvoid coalescence (1) surface nearly parallel to load axis and dominant primary slip twin systems, (2) step like fractured surfaces parallel and perpendicular to load axis and related to thickness of deformation bands (see Fig. 13)

Fig. [illegible] SEM [illegible]

[illegible] scopic shear bands can occur among grains with differing orientations from incompatibilities of critical stresses for slip and twin systems and the development of persistent [illegible] structural barriers across high angle grain boundaries. More importantly, the constraint of the deformation mechanisms within micro-shear bands, to less than a grain size scale, can lead to an effective grain refinement and further overall strain hardening [43].

Strain Localization, Strain Instability, and Fracture. The solution treatment temperature of 1030 to 1040 C used in this study dissolved many primary carbides that could initiate the particle decohesion or cracking, that leads to fracture [2,6,14,23,47]. The short time at temperature during high strain increment TMT reduces the amount of diffusion and also decreases precipitation of brittle, or incoherent carbides. High strain increments during TMT of Hadfield steel result in high stresses and strains, minimal recovery, twins, and deformation bands.

Micro size shear bands are plastic instabilities that can provide local softening and deformation when they propagate under stress by transformations leading to twinning, strain induced martensite, or the local multiplication of new dislocations [6,42-45,48]. Although shear became concentrated along some crystallographic systems and within bands at low strains (Figures 3,6,7), deformation continued with macroscopic and overall work hardening to high uniform strains (see Figures 2,8). Therefore, micro shear bands and their mechanisms do not appear to function as failure modes leading to necking and fracture in tension [14,23].

The fracture surface profile and scanning electron microscopy (SEM) micrograph of Figures 12-13 indicate a typical fracture initiation region is distinguished by grain boundary decohesion, microcracking, and cleavage. All tensile

tested specimens revealed similar but varied amounts of decohesion and/or cleavage mechanisms. Cleavage-like fractures (see Figure 12 b) along stepped and planar surfaces correlate to crystallographic features. A first example demonstrates facet-like cleavage with a fracture surface oriented nearly parallel to the load axis and the direction of shear flow on primary systems. A second example involves two kinds of facets, one parallel to the load axis and one with step-like fracture surfaces nearly perpendicular to the load axis and direction of shear flow. The fracture features of the second example are dependent upon the thickness of bands of twinned and slipped material. Similar cases of cleavage-like brittle fracture behavior are also shown together in the SEM micrograph of Figure 13. Microcrack growth, like plastic deformation, was often limited by crystallographic incompatibilities.

Surfaces in the fracture initiation region exhibit only limited amounts of microvoid growth and coalescence [6,47]. This is consistent with low fracture ductility. Boundaries of twinned material appear to influence the mechanisms of both ductile and cleavage-like fracture.

Unlike fracture initiation, the fracture surfaces and microvoids formed during final fracture are mainly transgranular, mostly unrelated to crystallographic systems or grain boundaries.

Conclusions

TMT and strain in tension can strengthen solution treated 16-18 HRC Hadfield steel to 56-57 HRC without plastic flow instability or fracture. Mechanical twinning occurs up to 454 °C. Mechanical property trends show TMT may be more beneficial in maintaining toughness and ductility than cold work to an equivalent hardness.

Acknowledgments

The author gratefully acknowledges support by M.R. Staker, other staff at Watertown, and assistance from Professor Biederman and staff at Worcester Polytechnic Institute with transmission electron microscopy.

References

1. Hadfields Ltd, *Manganese Steel*, Oliver and Boyd, London (1956)
2. ASM, *Properties and Selection: Stainless Steels, Tool Materials and Special Purpose Metals*. Metals Handbook, Vol. 3. ninth ed., pp. 568-588, ASM, Metals Park, Ohio (1980)
3. Doepkin, H.C., J. Met., Feb., 166-170 (1952)
4. Dieter, G.E., *Mechanical Metallurgy*, p.329, 2nd ed., McGraw-Hill, NY (1976)
5. Rama Rao, P. and V.V. Kutumbarao, Int. Rev. Met., 34, 69-86 (1989)
6. Meyers, M.A. and K.K. Chawla, *Mechanical Metallurgy Principles and Applications*, Prentice-Hall, Englewood Cliffs, N.J. (1984)
7. White, C.H. and R.W.K. Honeycombe, J. Iron Steel Inst., 200, 457-466 (1962)
8. Drobnjak, D.J. and J.G. Parr, Met. Trans., 1, 1521-1526 (1970)
9. Roberts, W.N. , Trans. Met. Soc. AIME, 230, 372-377 (1964)
10. Raghavan, K.S., A.S. Sastri, and M.J. Marcinkowski , Trans. Met. Soc. AIME, 245, 1569-1575 (1969)
11. Remy, L. and A. Pineau, Mat. Sci. Engr., 28, 99-107 (1977)
12. Olson, G.B., in *Deformation, Processing, and Structure*, pp. 391-424, ed. G. Krauss, ASM, Metals Park, OH (1984)
13. Adler, P.H., G.B. Olson, and W.S. Owen, Met. Trans. A, 17A, 1725-1737 (1986)
14. Hutchinson, J.W., Scr. Met., 18, 421-422 (1984)
15. Clifton, R.J. , J. Duffy, K.A. Hartley, and T. G. Shawki, Scr. Met., 18, 443-448 (1984)
16. Rogers, H.C. in *Deformation, Processing, and Structure*, p. 425, ed. G. Krauss, Metals Park Ohio (1984)
17. McElroy, R.J. and Z.C. Sckopiak, Int. Met. Rev., 17, 175-202 (1972)
18. Thompson, A.W., Met. Trans.A, 8A, 833-842 (1977)
19. Nishiyama, Z., M. Oka, and H. Nakagawa, Trans. JIM., 6, 88-92 (1962)
20. Dastur, Y.N. and W.C. Leslie, Met. Trans. A, 12A, 749-759 (1981)
21. Rémy, L., Met. Trans. A, 12A, 387-407 (1981)
22. Kandarpa, V. and J.W. Spretnak, Trans. Met. Soc. AIME, 245, 1439-1442 (1969)
23. Morris, J.W. Jr. and E.N.C. Dalder, J. Met., Oct., 24-33 (1985)
24. Cahn, J.W., Acta Met., 25, 1021-1026 (1977)
25. Kim, Y.G., J.M. Han, and J.S. Lee, Mat. Sci. Engr. A, A114, 51-59.(1989)
26. Cullity, B.D, *Elements of X-Ray Diffraction*, p. 508, 2nd ed., Addison-Wesley, Reading, MA (1978)
27. Subramanyam, D.K. , G.W. Grube, and H.J. Chapin, *Metallography and Microstructure*, Metals Handbook, Vol. 9, pp. 237-241, ASM, ninth ed. Metals Park, Ohio (1985)
28. Mori, T. and H. Fujita, Trans. JIM, 18, 17-24 (1977)
29. Blewitt, T.H., R.R. Coltman, and J.K. Redman, J. Apl. Phys., 28, 651-660 (1957)
30. Suzuki, H. and C.S. Barrett, Acta Met., 6, 156-165 (1958)
31. Kestenbach, H.J., Phil. Mag., 36, 1509-1515 (1977)
32. Blicharski, M. and S. Gorczyca, Met. Sci., July, 303-312 (1978)
33. Aaronson, H.I., T. Furuhara, J.M. Rigsbee, W.T. Reynolds, Jr., and J.M. Howie, Met. Trans. A, 21A, 2369-2409 (1990)
34. Hirsch, P.B., A. Howie, R.B. Nicholson, D.W. Pashley, and M.J. Whelan, *Electron Microscopy of Thin Crystals*, p. 141, Butterworths, London (1965)
35. Thomas, G. and M. J. Goringe, *Transmission Electron Microscopy of Materials*, pp. 94-100, John Wiley and Sons, Inc., New York (1979)
36. Murr, L.E., *Electron and Ion Microscopy and Microanalysis*, Marcel Dekker, NY (1982)
37. Champion, A.R. and R.W. Rohde, J. Appl. Phys., 41, 2213-2222 (1970)
38. Goodchild, D., W.T. Roberts, and D.V. Wilson, Acta Met., 18, 1137-1145 (1970)
39. Lagneborg, R., Acta Met., 12, 823-843 (1964)
40. Dash, J., and H.M. Otte, in *Electron Microscopy*, ed. S.S. Breese, Academic Press, Philadelphia, PA, p. HH-4, (1962)
41. Hatherly, M. and A.S. Malin, Scr. Met., 18, 449-454 (1984)
42. Asaro, R.J. and A. Needleman, Scr. Met., 18, 429-435 (1984)

43. Duggan, B.J., M. Hatherly, W.B. Hutchinson, and P.T. Wakefield, Met. Sci., 12, 343-351 (1978)
44. Morii, K. and Y. Nakayama, Trans. JIM, 22, 857-864 (1981)
45. Suzuki, T., H. Kojima, K. Suzuki, T. Hashimoto, and M. Ichihara, Acta Met., 25, 1151-1162 (1977)
46. Olson, G. B. and M. Cohen, Met. Trans. A, 6A, 791-795 (1975)
47. Luong, L.H.S. and R. H. Brown, Trans. ASME, 103, 431-436 (1981)
48. Argon, A.S., in *The Inhomogeneity of Plastic Deformation*, pp. 181, ASM, Metals Park, OH (1973)

DISTRIBUTION LIST

No. of Copies	To
1	Office of the Under Secretary of Defense for Research and Engineering, The Pentagon, Washington, DC 20301
	Director, U.S. Army Research Laboratory, 2800 Powder Mill Road, Adelphi, MD 20783-1197
1	ATTN: AMSRL-OP-CI-AD, Technical Publishing Branch
1	AMSRL-OP-CI-AD, Records Management Administrator
	Commander, Defense Technical Information Center, Cameron Station, Building 5, 5010 Duke Street, Alexandria, VA 23304-6145
2	ATTN: DTIC-FDAC
1	MIAC/CINDAS, Purdue University, 2595 Yeager Road, West Lafayette, IN 47905
	Commander, Army Research Office, P.O. Box 12211, Research Triangle Park, NC 27709-2211
1	ATTN: Information Processing Office
	Commander, U.S. Army Materiel Command, 5001 Eisenhower Avenue, Alexandria, VA 22333
1	ATTN: AMCSCI
	Commander, U.S. Army Materiel Systems Analysis Activity, Aberdeen Proving Ground, MD 21005
1	ATTN: AMXSY-MP, H. Cohen
	Commander, U.S. Army Missile Command, Redstone Arsenal, AL 35809
1	ATTN: AMSMI-RD-CS-R/Doc
	Commander, U.S. Army Armament, Munitions and Chemical Command, Dover, NJ 07801
2	ATTN: Technical Library
	Commander, U.S. Army Natick Research, Development and Engineering Center, Natick, MA 01760-5010
1	ATTN: Technical Library
	Commander, U.S. Army Satellite Communications Agency, Fort Monmouth, NJ 07703
1	ATTN: Technical Document Center
	Commander, U.S. Army Tank-Automotive Command, Warren, MI 48397-5000
1	ATTN: AMSTA-ZSK
1	AMSTA-TSL, Technical Library
	Commander, White Sands Missile Range, NM 88002
1	ATTN: STEWS-WS-VT
	President, Airborne, Electronics and Special Warfare Board, Fort Bragg, NC 28307
1	ATTN: Library
	Director, U.S. Army Research Laboratory, Weapons Technology, Aberdeen Proving Ground, MD 21005-5066
1	ATTN: AMSRL-WT
	Commander, Dugway Proving Ground, UT 84022
1	ATTN: Technical Library, Technical Information Division
	Commander, U.S. Army Research Laboratory, 2800 Powder Mill Road, Adelphi, MD 20783
1	ATTN: AMSRL-SS

No. of Copies	To
	Director, Benet Weapons Laboratory, LCWSL, USA AMCCOM, Watervliet, NY 12189
1	ATTN: AMSMC-LCB-TL
1	AMSMC-LCB-R
1	AMSMC-LCB-RM
1	AMSMC-LCB-RP
	Commander, U.S. Army Foreign Science and Technology Center, 220 7th Street, N.E., Charlottesville, VA 22901-5396
3	ATTN: AIFRTC, Applied Technologies Branch, Gerald Schlesinger
	Commander, U.S. Army Aeromedical Research Unit, P.O. Box 577, Fort Rucker, AL 36360
1	ATTN: Technical Library
	U.S. Army Aviation Training Library, Fort Rucker, AL 36360
1	ATTN: Building 5906-5907
	Commander, U.S. Army Agency for Aviation Safety, Fort Rucker, AL 36362
1	ATTN: Technical Library
	Commander, Clarke Engineer School Library, 3202 Nebraska Ave., N, Fort Leonard Wood, MO 65473-5000
1	ATTN: Library
	Commander, U.S. Army Engineer Waterways Experiment Station, P.O. Box 631, Vicksburg, MS 39180
1	ATTN: Research Center Library
	Commandant, U.S. Army Quartermaster School, Fort Lee, VA 23801
1	ATTN: Quartermaster School Library
	Naval Research Laboratory, Washington, DC 20375
2	ATTN: Dr. G. R. Yoder - Code 6384
	Chief of Naval Research, Arlington, VA 22217
1	ATTN: Code 471
	Commander, U.S. Air Force Wright Research & Development Center, Wright-Patterson Air Force Base, OH 45433-6523
1	ATTN: WRDC/MLLP, M. Forney, Jr.
1	WRDC/MLBC, Mr. Stanley Schulman
	U.S. Department of Commerce, National Institute of Standards and Technology, Gaithersburg, MD 20899
1	ATTN: Stephen M. Hsu, Chief, Ceramics Division, Institute for Materials Science and Engineering
1	Committee on Marine Structures, Marine Board, National Research Council, 2101 Constitution Avenue, N.W., Washington, DC 20418
1	Materials Sciences Corporation, Suite 250, 500 Office Center Drive, Fort Washington, PA 19034
1	Charles Stark Draper Laboratory, 555 Technology Square, Cambridge, MA 02139
	Wyman-Gordon Company, Worcester, MA 01601
1	ATTN: Technical Library

No. of Copies	To
	General Dynamics, Convair Aerospace Division, P.O. Box 748, Fort Worth, TX 76101
1	ATTN: Mfg. Engineering Technical Library
	Plastics Technical Evaluation Center, PLASTEC, ARDEC, Bldg. 355N, Picatinny Arsenal, NJ 07806-5000
1	ATTN: Harry Pebly
1	Department of the Army, Aerostructures Directorate, MS-266, U.S. Army Aviation R&T Activity - AVSCOM, Langley Research Center, Hampton, VA 23665-5225
1	NASA - Langley Research Center, Hampton, VA 23665-5225
	U.S. Army Vehicle Propulsion Directorate, NASA Lewis Research Center, 2100 Brookpark Road, Cleveland, OH 44135-3191
1	ATTN: AMSRL-VP
	Director, Defense Intelligence Agency, Washington, DC 20340-6053
1	ATTN: ODT-5A (Mr. Frank Jaeger)
	Director, U.S. Army Research Laboratory, Watertown, MA 02172-0001
2	ATTN: AMSRL-OP-CI-D, Technical Library
5	Author